Magnetic properties and crystal structure of Sr3CoIrO6and Sr3NiIrO6

MIKHAILOVA, D., SCHWARZ, B., SENYSHYN, A., BELL, Anthony <http://orcid.org/0000-0001-5038-5621>, SKOURSKI, Y., EHRENBERG, H., TSIRLIN, A.A., AGRESTINI, S., ROTTER, M., REICHEL, P., CHEN, J.M., HU, Z., LI, Z.M., LI, Z.F. and TJENG, L.H.

Citation:

Copyright and re-use policy

Magnetic properties and crystal structure of Sr₃CoIrO₆ and Sr₃NiIrO₆

D. Mikhailova,[1,2] B. Schwarz,[2] A. Senyshyn,[3] A. M. T. Bell,[4] Y. Skourski,[5] H. Ehrenberg,[2,6] A. A. Tsirlin,[1] S. Agrestini,[1]
M. Rotter,[1] P. Reichel,[1,2] J. M. Chen,[7] Z. Hu,[1] Z. M. Li,[7] Z. F. Li,[7] and L. H. Tjeng[1]

[1]*Max Planck Institute for Chemical Physics of Solids, Nöthnitzer Str. 40, D-01187 Dresden, Germany*
[2]*Institute for Complex Materials, IFW Dresden, Helmholtzstr. 20, D-01069 Dresden, Germany*
[3]*Forschungs-Neutronenquelle Heinz Maier-Leibnitz (FRM-II), Technische Universität München, Lichtenbergstr. 1,
D-85747 Garching near München, Germany*
[4]*Hamburger Synchrotronstrahlungslabor am Deutschen Elektronen-Synchrotron, Notkestr. 85, D-22607 Hamburg, Germany*
[5]*Dresden High Magnetic Field Laboratory, Forschungszentrum Dresden–Rossendorf, D-01314 Dresden, Germany*
[6]*Karlsruhe Institute of Technology (KIT), Institute for Applied Materials (IAM), Hermann-von-Helmholtz-Platz 1,
D-76344 Eggenstein-Leopoldshafen, Germany*
[7]*National Synchrotron Radiation Research Center (NSRRC), 101 Hsin-Ann Road, Hsinchu 30077, Taiwan*

We have studied the magnetic properties and crystal structure of Sr₃CoIrO₆ and Sr₃NiIrO₆ as a function of temperature. Two characteristic temperatures, $T_1 = 90$ K and $T_2 = 25$ K for Sr₃CoIrO₆, and $T_1 = 85$ K and $T_2 = 15$ K for Sr₃NiIrO₆, were observed. Below T_1 a significant increase of magnetization and below T_2 a weak temperature dependence of magnetization in the field-cooled and practically zero magnetization values in the zero-field-cooled mode were detected for both compounds. The existence of Ir⁴⁺ in Sr₃CoIrO₆ was confirmed by an Ir-L_{III} x-ray absorption measurement. Magnetoelastic effects have been observed in the temperature dependence of the lattice parameters of Sr₃CoIrO₆ and Sr₃NiIrO₆. The magnetic structure of Sr₃CoIrO₆ in zero fields can be described as a commensurate modulated antiferromagnet with a propagation vector $\mathbf{k} = (0,0,1)$. Neutron powder diffraction with polarized neutrons gave evidence of short-range magnetic order, above and below the magnetic ordering temperature.

PACS number(s): 75.25.−j, 71.70.Ej, 61.05.fm

I. INTRODUCTION

Among numerous isostructural phases with $A_3MM'O_6$ stoichiometry (M and M' are transition metals), six of them, Ca₃Co₂O₆,[1,2] Ca₃CoRhO₆,[3–8] Ca₃CoIrO₆,[9,10] Sr₃NiRhO₆,[11] Sr₃NiIrO₆,[12,13] and the recently reported Sr₃Co₂O₆,[14] seem to exhibit similar magnetic behavior. This is surprising considering the different magnetic cations and their different electronic states. For example, in Ca₃Co₂O₆, the presence of both high-spin Co³⁺ (HS-Co³⁺, d^6, $S = 2$) and nonmagnetic low-spin Co³⁺ (LS-Co³⁺, d^6, $S = 0$) states was established.[15,16] A similar scenario can be envisaged for Sr₃Co₂O₆. On the other hand, a HS-Co²⁺ (d^7, $S = 3/2$) state in combination with LS-Rh⁴⁺ (d^5, $S = 1/2$) and LS-Ir⁴⁺ (d^5, $S = 1/2$) configurations were determined for Ca₃CoRhO₆[7,17] and Ca₃CoIrO₆,[10] respectively. Moreover, HS-Ni²⁺ (d^8, $S = 1$) and LS-Ir⁴⁺/LS-Rh⁴⁺ states were deduced for Sr₃NiIrO₆[12]/Sr₃NiRhO₆.[11]

The crystal structure of these compounds is built of chains of face-sharing MO_6 trigonal prisms (M = Co, Ni) and $M'O_6$ octahedra (M' = Co, Rh, Ir, Mn) stacked along the c axis. The chains are separated by Sr or Ca cations and form a triangular lattice. The magnetism of these compounds can be characterized by two temperatures: (1) below T_1 a complex antiferromagnetic order appears and magnetic phase transitions in applied field lead to a nonlinear evolution of the magnetization; (2) below $T_2 < T_1$ a spin-freezing state was proposed. Note that for Ca₃CoIrO₆ only a spin-freezing temperature T_2 was reported.[10]

For Ca₃Co₂O₆ and Ca₃CoRhO₆ a partially disordered antiferromagnetic (PDA) interchain and a ferromagnetic intrachain Co type of order were observed by neutron diffraction.[2,4] Replacement of octahedrally coordinated LS-

Co³⁺ in Ca₃Co₂O₆ by LS-Rh⁴⁺ increases the magnetic ordering temperature T_1 from 25 to 90 K.

Sr₃CoIrO₆ has been recently synthesized for the first time[18] and is isostructural to the materials discussed previously. Thus magnetic properties similar either to Ca₃CoRhO₆ or to Ca₃CoIrO₆ can be expected. By comparing Ca₃CoRhO₆, Ca₃CoIrO₆, Sr₃NiIrO₆, and Sr₃CoIrO₆ it is possible to disentangle the influence of different degrees of freedom such as electronic configuration (d^7 for Co²⁺ and d^8 for Ni²⁺) or spin state and geometric criteria such as the interchain distances due to the different cation radii of Ca²⁺/Sr²⁺. The magnetic 4d- and 5d-cations Rh and Ir contribute a much smaller magnetic moment than Co and Ni. Up to now, only for Ca₃CoRhO₆ magnetic Bragg reflections were observed by neutron powder diffraction below T_1.[3,4] At temperatures down to T_2, a PDA state was inferred. In the magnetic phase 2/3 of the ferromagnetic chains are coupled antiferromagnetically while the other 1/3 of the chains stays disordered, with a spin orientation along the c axis either in "positive" or "negative" direction.[4] This exotic magnetic state might be the consequence of an antiferromagnetic interchain interaction on the triangular lattice and has been discussed for Ca₃CoRhO₆ and Sr₃NiIrO₆. An even more complex glassy-type magnetic behavior without PDA was proposed for Ca₃CoIrO₆.[10] For a field-oriented crystalline sample of Ca₃CoRhO₆ a saturated magnetization of about 4 μ_B/formula units (f.u.) was observed at 4 T between T_2 and T_1, corresponding to a ferromagnetic alignment of HS-Co²⁺ and LS-Rh⁴⁺ on all three chains.[3] A very large orbital magnetic moment of HS-Co²⁺ ions of about 1.7 μ_B was predicted theoretically[15] and found in Ca₃CoRhO₆ by x-ray absorption and x-ray magnetic dichroism experiments.[17]

In contrast, for Ca_3CoIrO_6[10] and Sr_3NiIrO_6[12] the magnetization does not saturate even at much higher fields. Differences in the magnetic behavior of $Ca_3Co_2O_6$, Ca_3CoRhO_6, and Ca_3CoIrO_6 were attributed to the different strengths of magnetic interchain and intrachain interactions, which are reflected by the c/a ratio of the underlying crystal structure.[10] The c/a ratio increases in the series $Ca_3CoM'O_6$ from 1.143 ($M' =$ Co) via 1.166 ($M' =$ Rh) to 1.189 ($M' =$ Ir). However, this is a very simplified view in the light of the complex interchain magnetic exchange interactions, as discussed, for example, for $Ca_3Co_2O_6$ in Ref. 2.

In the present work we studied two compounds, Sr_3CoIrO_6 and Sr_3NiIrO_6, which are very close from the crystallographic point of view but different in their electronic configuration. Magnetic properties have been measured in static and pulsed magnetic fields up to 60 T between 1.8 and 350 K. The temperature evolution of the lattice parameters was determined by synchrotron powder diffraction, and the time dependence of the magnetization process was studied at temperatures near the spin-freezing transition at T_2. Powder diffraction measurements using unpolarized, and polarized neutron beams from room temperature down to 4 K were performed on Sr_3CoIrO_6.

II. EXPERIMENTAL

A. Synthesis and sample characterization

Sr_3MIrO_6 samples were prepared by solid state reactions in an Ar atmosphere at 1473 K for 24 h from stoichiometric powder mixtures of CoO for $M =$ Co and NiO for $M =$ Ni (Alfa Aesar, 99.999%) with IrO_2 (Umicore) and $SrCO_3$ (Alfa Aesar, 99.99%).[18] The phase analysis and the determination of unit cell parameters was based on x-ray powder diffraction (XPD) done on a STOE STADI P diffractometer (Co-$K\alpha_1$-radiation) in flat-sample transmission mode. The Sr_3CoIrO_6 contained a tiny amount of metallic Ir (0.8 wt.%) that does not affect any of the results presented subsequently. The Sr_3NiIrO_6 sample was single phase.

B. X-ray absorption spectroscopy

The Ir-L_{III} x-ray absorption spectra (XAS) of Sr_3CoIrO_6 and of an Ir^{4+} reference compound Sr_3ZnIrO_6, prepared according to Ref. 19, were recorded at the 01C beamline of the National Synchrotron Radiation Research Center (NSRRC) in Taiwan, which is equipped with a double-crystal Si(111) monochromator. Both Ir-L_{III} spectra were collected under identical conditions applying the bulk sensitive fluorescence yield method using a Lytle detector. The photon energy resolution for the present set-up was 1.5 eV at the Ir-L_{III} edge ($\sim$11,218 eV), for energy calibration the L_{III} edge of Pt (at 11,564 eV) was used.

C. Magnetic measurements

The temperature dependence of the magnetization was measured both in zero-field-cooled (ZFC) and in field-cooled (FC) mode between $T = 1.8$ and 350 K. The field dependence of the magnetization up to 9 T was determined using a magnetic property measurement system MPMS XL7 equipped with a SQUID magnetometer (Quantum Design Company) and with a vibrating sample magnetometer (VSM) in a physical property measurement system PPMS 6000 (Quantum Design Company). The time dependence of the magnetization was measured at 6 T in the temperature range between 21 and 30 K for Sr_3CoIrO_6 and between 12.5 and 14 K for Sr_3NiIrO_6.

Magnetization measurements in pulsed magnetic fields were performed at the Dresden High Magnetic Field Laboratory (Forschungszentrum Dresden–Rossendorf) using a pulsed magnet powered by a 1.44 MJ capacitor bank.[20] With an inner bore of 20 mm, the magnet yielded fields up to 60 T with a rise time of 7 ms and a total pulse duration of about 20 ms. All measurements were performed twice, with and without the sample, in order to remove the background signal contribution. All the data were collected at a temperature of 50 K.

D. Low-temperature synchrotron powder diffraction

The crystal structures of Sr_3CoIrO_6 and Sr_3NiIrO_6 in the temperature range of 9–300 K were determined by synchrotron powder diffraction at the beamline B2[21] at HASYLAB/DESY (Hamburg, Germany). The investigations were performed in a quartz capillary in a He atmosphere in Debye–Scherrer mode using the onsite readable image-plate detector OBI[22] and a He closed-cycle cryostat. The synchrotron x-ray wavelengths used for each sample were 0.53837 Å (Sr_3CoIrO_6) and 0.53922 Å (Sr_3NiIrO_6).

E. Low-temperature neutron powder diffraction

Elastic coherent neutron scattering experiments were performed in zero field on the high-resolution structure powder diffractometer (SPODI) at the research reactor FRM-II (Garching, Germany) with monochromatic neutrons of 1.5481(1) Å wavelength.[23] Measurements were performed in Debye–Scherrer geometry. The powder sample (*ca*. 1 cm^3 in volume) was filled into a thin-wall (0.15 mm) vanadium can of 10-mm diameter and then mounted in a top-loading closed-cycle refrigerator, which was cooled down from room temperature to 4 K in five hours. Helium 4 was used as a heat transmitter. The temperature was measured using two Cernox thin-film resistance cryogenic temperature sensors and controlled by a temperature controller from LakeShore. Powder diffraction data were collected between 4 and 70 K and then corrected for geometrical aberrations and the curvature of the Debye–Scherrer rings. The collecting time for a typical diffraction pattern was five hours.

Experiments with polarized neutrons have been carried out with the DNS spectrometer (Jülich Centre for Neutron Science [JCNS], FRM-II reactor). An unambiguous separation of nuclear coherent, spin incoherent, and magnetic scattering contributions over a wide scattering angle has been achieved by neutron polarization analysis applying the well-established *xyz* method.[24] The experiment was carried out at two temperatures, 4 and 80 K, using monochromatic neutrons with a wavelength of 4.74 Å. The polarization of the neutron beam was better than 96%.
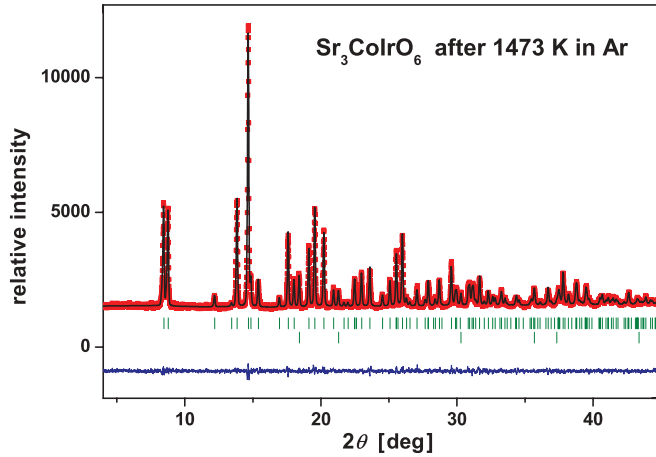
FIG. 1. (Color online) Room temperature x-ray diffraction pattern of Sr_3CoIrO_6, prepared at 1473 K in an Ar atmosphere, observed, and calculated profiles, based on the Rietveld refinement of a structure model derived from the K_4CdCl_6 structure, together with their difference curve. Tick marks represent, from top to bottom, the positions of reflections for Sr_3CoIrO_6 [R-$3c$, $a = 9.62112(9)$ Å, $c = 11.1541(1)$ Å] and metallic Ir (Fm-$3m$, 1% w/w).

F. Heat capacity

The heat capacity was measured between 10 and 150 K for Sr_3CoIrO_6 and between 4 and 250 K for Sr_3NiIrO_6 in zero magnetic field with a standard puck in a PPMS (Quantum Design) applying the relaxation method with 2% temperature rise.

III. RESULTS AND DISCUSSION

A. Crystal structures of Sr_3MIrO_6 ($M = $ Co, Ni)

The XRD pattern of Sr_3CoIrO_6 and a Rietveld refinement is presented in Fig. 1. The Sr_3MIrO_6 structure contains one-dimensional chains along the c direction consisting of alternating face-sharing MO_6 trigonal prisms and IrO_6 octahedra (Fig. 2). The chains are separated by Sr cations. Each Co-Ir chain is shifted relatively to three nearest-neighbor chains by $z = 1/3$ and relatively to the other nearest-neighbor chains by $z = 2/3$ (Fig. 2). This means that the phase of each chain is shifted relatively to three nearest-neighbor chains by 60° and to the other three nearest-neighbor chains by 120° toward the c axis. The lattice parameters are $a = 9.62112(9)$ Å and

$c = 11.1541(1)$ Å. The intrachain Co-Co distance in Sr_3CoIrO_6 is 5.577 Å and between the chains is 5.857 Å. Sr_3NiIrO_6 is isostructural to Sr_3CoIrO_6 with the lattice parameters $a = 9.6188(2)$ Å, $c = 11.2004(3)$ Å, the intrachain Ni-Ni distance of 5.600 Å, and the interchain distance of 5.859 Å (XRD data are not shown).

In contrast to the $Ca_3Co_{1+x}Ir_{1-x}O_6$-system,[9] in which the whole series from x(Co) $= 0$ to x(Co) $= 1$ exists, attempts to synthesize $Sr_3Co_{1.5}Ir_{0.5}O_6$ led to a mixture of (i) $Sr_3Co_{2-x}Ir_xO_6$ [R-$3c$, $a = 9.6149(3)$ Å, $c = 11.1370(5)$ Å)]; (ii) cubic $Sr_2Co_{1-x}Ir_xO_6$ with a perovskite-type structure [Fm-$3m$, $a = 7.8351(2)$ Å]; and (iii) a small amount of metallic Ir. Some differences in lattice parameters of isostructural Sr_3CoIrO_6 and $Sr_3Co_{2-x}Ir_xO_6$ enabled us to propose a small Co/Ir nonstoichiometry in our samples. A slight occupancy of Co on the respective Ir site (less than 3%) was also found by a Rietveld refinement of Sr_3CoIrO_6 and explains the presence of metallic Ir impurities (less than 1% w/w) in the sample. Note that a significant cation mixing can cause a huge change in the magnetic behavior, as found for the closely related Sr_3ZnRhO_6. In fact, Sr_3ZnRhO_6 with a commensurate crystal structure presents a clear long-range magnetic ordering at 16 K, as confirmed by heat capacity and neutron powder diffraction measurements.[25] On the other hand, the compound of the same composition with an incommensurate crystal structure and the mixed occupancy of octahedral and prismatic sites by Zn, Rh, and Sr cations shows a Curie–Weiss-like behavior down to 2 K.[26]

B. X-ray absorption spectroscopy study of Sr_3CoIrO_6

In order to determine the valence of Ir in Sr_3CoIrO_6 we performed Ir-L_{III} XAS investigations of Sr_3CoIrO_6 together with isostructural Sr_3ZnIrO_6 as a reference compound for Ir^{4+}.

It is well known that the white line position in the Ir-L_{III} edge is shifted to higher energy by more than one eV with an increase in the formal valence of Ir ion from $3 +$ to $4 +$.[27,28] In Fig. 3 we compare the Ir-L_{III} absorption spectra of Sr_3CoIrO_6 and Sr_3ZnIrO_6. Since the white line position of both compounds lies at the same energy, the existence of an Ir^{4+}/Co^{2+} valence state can be inferred. Moreover, the very similar near-edge spectral structures indicate the same local environment for both materials. Note that the existence of Ir^{3+} in complex oxides is rather unlikely and has only been mentioned for Sr_2MIrO_6 ($M = $ Nb, Ta) perovskites.[29]

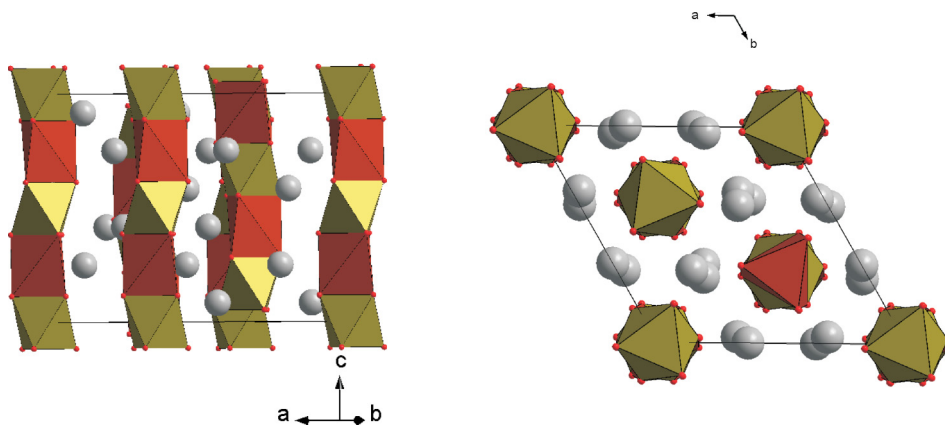FIG. 2. (Color online) Crystal structure of Sr_3CoIrO_6 presenting one-dimensional chains along the c direction consisting of alternating face-sharing CoO_6 trigonal prisms and IrO_6 octahedra (left). Grey spheres are Sr atoms. A projection of one unit cell on the ab plane is shown (right).
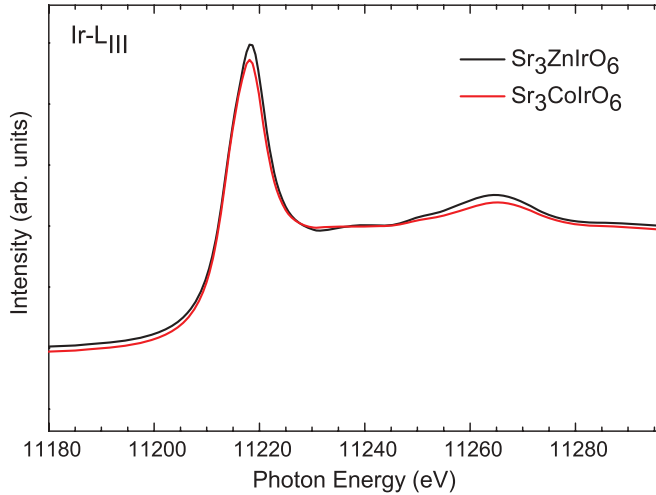
Ir-L$_{III}$

FIG. 3. (Color online) Ir L_{III}-edge XAS in the white line region, for Sr_3ZnIrO_6 as a standard for Ir^{+4} (black line) and Sr_3CoIrO_6 (red/dark gray line).

C. Magnetic characterization

1. Temperature dependence of magnetization

The temperature dependences of the magnetization for $M = Co$ and Ni in an external magnetic field of 0.05 T are similar [see Fig. 4(a)]. A significant difference between FC and ZFC measurements points to the appearance of a ferro- or ferrimagnetic component at low temperature. For each phase, two characteristic temperatures, $T_1 = 90$ K and $T_2 = 25$ K for Co, and $T_1 = 85$ K and $T_2 = 15$ K for Ni (see inset in Fig. 4), are observed. Below T_1 a significant increase of magnetization can be seen, and below T_2 a weak temperature dependence of magnetization in the FC and practically zero magnetization values in ZFC mode were detected. The same two characteristic temperatures were also observed in the significantly smaller magnetic field of 0.005 T (data not shown here). While for Ca_3CoRhO_6 two characteristic temperatures $T_1 = 90$ K and $T_2 = 30$ K were observed, only one temperature corresponding to the onset of a large difference between FC and ZFC was detected for Ca_3CoIrO_6.[10]

For Sr_3NiIrO_6 we observe a spin-freezing temperature $T_2 \sim$ 15 K (Fig. 4), which is similar to the results reported in Refs. 12 and 19. The authors of Ref. 12 have discussed the magnetic behavior of Sr_3NiIrO_6 in low magnetic fields between T_1 and T_2 as a PDA state, corresponding to the coexistence of 2/3 antiferromagnetically coupled ferrimagnetic chains with antiferromagnetic intrachain coupling between Ni^{2+} ($S = 1$) and Ir^{4+} ($S = \frac{1}{2}$) and 1/3 magnetically incoherent chains in a triangular lattice. However, it has to be noted that in the neutron diffraction pattern no evidence for antiferromagnetic order could be seen.[19] Antiferromagnetic coupling between Ni^{2+} and Ir^{4+} was postulated based (i) on the negative Curie–Weiss temperature in the paramagnetic region, (ii) low magnetization values and the absence of saturation even in the field of 35 T,[12] and (iii) supported by theoretical calculations.[13]

We analyzed the temperature dependence of the reciprocal molar magnetic susceptibility of Sr_3NiIrO_6 in the paramagnetic region above 200 K applying a Curie–Weiss law Eq. (1) and found a paramagnetic moment of 3.50(1) μ_B per f.u. The

Curie–Weiss temperature $\theta = -33(5)$ K indicates a dominant antiferromagnetic interaction [Fig. 4(b)],

$$\frac{1}{\chi(T)} = \frac{3k_B(T - \theta)}{\mu_{eff}^2} = \frac{1}{\chi_0(T)} - \lambda. \quad (1)$$

In contrast to Sr_3NiIrO_6, our magnetization data of Sr_3CoIrO_6, fitted by the Curie–Weiss equation Eq. (1) between 250 and 400 K, revealed a positive Curie–Weiss temperature $\theta = 178(3)$ K and a paramagnetic moment of 4.36(1) μ_B per f.u.

Here we would like to make a note of caution. In principle, one has to be careful in applying the equation Eq. (1) for analyzing the paramagnetic susceptibility and drawing conclusions about the magnitude of magnetic moments and interactions in Co^{2+}-containing materials:[15–17,30] the degeneracy of the crystal field split states of a d^7 configuration may be lifted by the spin-orbit interaction, leading to nontrivial temperature dependence of the magnetic susceptibility. To what extent this is the case for Sr_3CoIrO_6 will be subject of a further study looking into the details of the electronic structure of this material.

2. Field dependence of magnetization

The field dependence of the magnetization of Sr_3MIrO_6 was systematically investigated between 10 and 90 K for $M = Co$ and between 5 and 55 K for $M = Ni$ with steps of 10 K. Each hysteresis curve was started and finished at 9 T for $M = Co$ and 6 T for $M = Ni$. After each measurement the field was switched off, and the sample was heated to the paramagnetic state above 100 K and cooled down without field to the next temperature. For Sr_3CoIrO_6 a saturation in the magnetization value of about 2.2 μ_B/f.u. was observed above 4 T for temperatures between 30 and 90 K (Fig. 5). Below 60 K an additional plateau at about 0.7 μ_B located between 0.5 and 1.8 T becomes visible. Below 30 K a quite different behavior without any saturation was observed (see Fig. 5).

Completely different magnetic hysteresis curves at 15 K for Sr_3CoIrO_6 were observed (Fig. 6) depending on whether the sample was cooled down without or with applied magnetic field. No saturation behavior and zero hysteresis loop was observed for the state after cooling down in zero field, while a hysteresis with saturated magnetization values, asymmetrically extended with respect to the magnetization axis, has been seen after cooling down in a magnetic field of 1 T. This difference in the magnetic behavior reflects the slow-spin dynamics below 25 K for Sr_3CoIrO_6 and resembles the frozen F-PDA state of Ca_3CoRhO_6.[3–5]

Applying pulsed magnetic fields up to 60 T at 50 K led also to a magnetic saturation with 2.2 μ_B/f.u. (see Fig. 7). Note that an almost saturated magnetization of 4.05 μ_B/f.u. parallel to the c axis was observed for the Ca_3CoRhO_6 polycrystalline sample, field-oriented along the c axis at $\sim$19 T and 70 K.[3] Due to strong magnetocrystalline anisotropy in such quasi-one-dimensional systems, the magnetization perpendicular to the easy c axis in Ca_3CoRhO_6 is much lower (0.53 μ_B/f.u. at $\sim$19 T and 70 K) and not saturated.[3] For a disordered Sr_3CoIrO_6 sample with random distribution of crystallites we can assume that about 1/3 of all
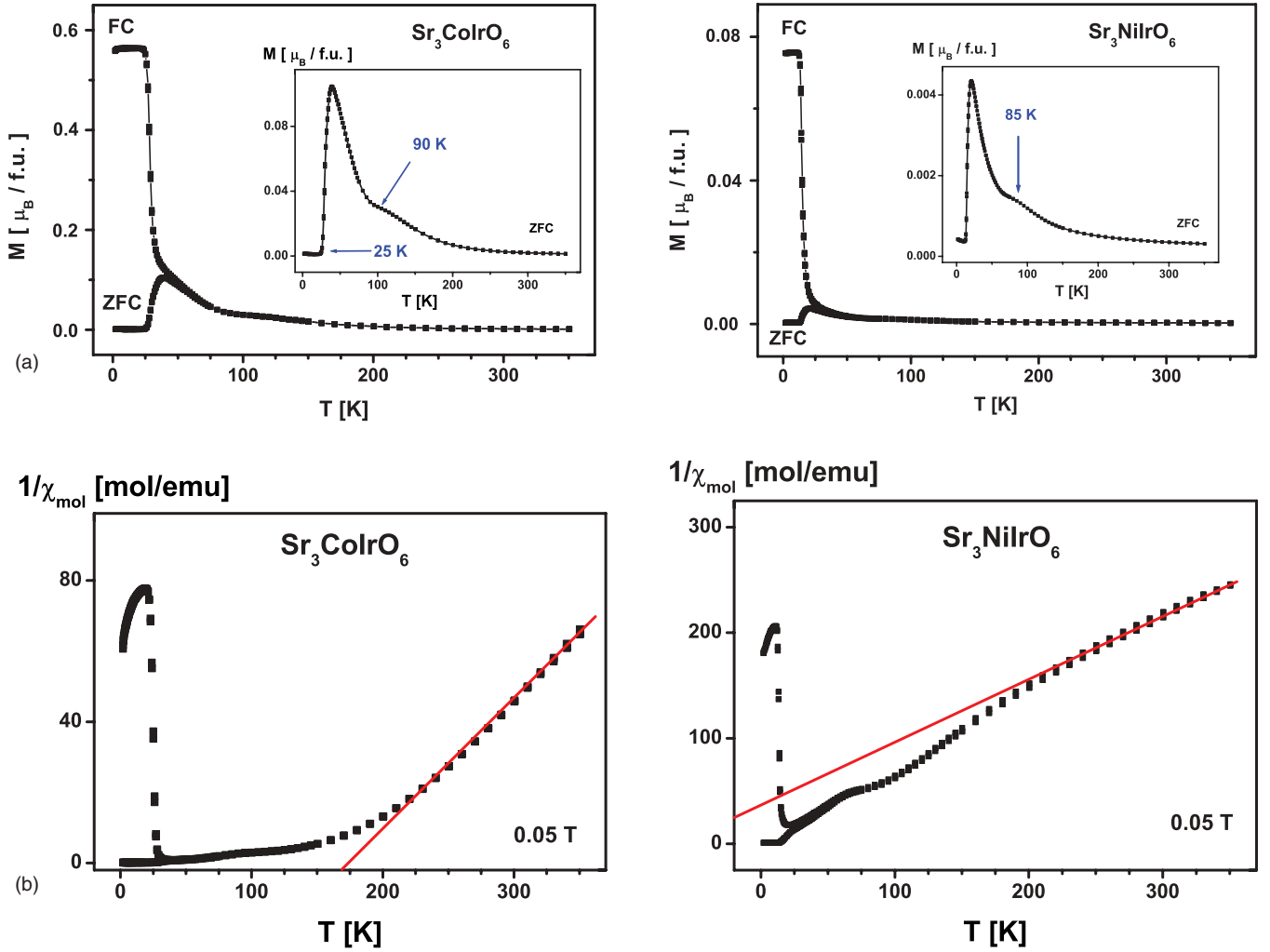
FIG. 4. (Color online) (a) Temperature dependence of magnetization at 0.05 T for Sr_3CoIrO_6 and Sr_3NiIrO_6. A significant increase of magnetization below $T_1 = 90$ K for the Co phase and below $T_1 = 85$ K for the Ni phase was observed, see inset. In FC mode the samples were cooled down in a magnetic field of 0.1 T and measured at 0.05 T. (b) Temperature dependence of reciprocal molar magnetic susceptibility at 0.05 T for Sr_3CoIrO_6 and Sr_3NiIrO_6. The drawn lines correspond to Curie–Weiss fits to the paramagnetic regions.

crystallites are oriented with the c axis along the magnetic field and deliver the largest contribution to the magnetization below the phase transition temperature. The plateau in magnetization between 0.5 and 1.8 T at 50 K will then correspond to $\sim$2.1 μ_B/f.u., and the saturation above 4 T to $\sim$6.6 μ_B/f.u. for a single crystal oriented along the easy c axis. A spin-only model would lead to a magnetization of 4 μ_B/f.u. only: $M/\mu_B = 2*(S_{Co(II)} + S_{Ir(IV)})$ with $S_{Co(II)} = 3/2$ and $S_{Ir(IV)} = 1/2$. The 6.6 μ_B value therefore indicates that the Co^{2+} ions must carry a significant orbital moment, well in line with the strong magnetocrystalline anisotropy. The plateau between 0.5 and 1.8 T could correspond to the ferrimagnetic ordering of Ir^{4+} and Co^{2+} ions, where 2/3 of the magnetic chains have all the spins parallel to the magnetic field and the other 1/3 has all the spins antiparallel.

The observed hysteresis in the magnetization up to 15 T (Fig. 7) in pulsed magnetic fields is probably due to the slow kinetics of spin orientations. Note that the measured magnetization of disordered Ca_3CoRhO_6 polycrystalline sample is far from the saturation.[31]

For our disordered polycrystalline sample of Sr_3NiIrO_6, a tendency for a plateau in the magnetization with $\sim$0.2 μ_B/f.u. can be seen at 15 K for fields above 5 T. At higher temperatures this tendency disappears completely (see Fig. 8). A coercive field of $\mu_0H = 0.25$ T was determined at 15 K. Below 15 K a more linear behavior with much smaller magnetization values without a significant coercivity were observed. At 15 K, a plateau at 5 T with a magnetization of 0.15 μ_B/f.u. in static magnetic field was reported in Ref. 12.

Assuming a magnetocrystalline anisotropy also for Sr_3NiIrO_6, we expect from our experiment a magnetization value of about $\sim$0.6 μ_B/f.u. at 15 K for a single crystal sample oriented along the c axis. The magnetization value for antiferromagnetic alignment of Ni^{2+} and Ir^{4+} ions in the chains, which was proposed in the work[13] based on density functional theory calculations, would be of 1.0 μ_B/f.u. considering only spin contributions: $M = 2[1/3(S_{Ni(II)} - S_{Ir(IV)}) + 1/3(S_{Ni(II)} - S_{Ir(IV)}) + 1/3(S_{Ni(II)} - S_{Ir(IV)})]$ with $S_{Ni(II)} = 1$ and $S_{Ir(IV)} = 1/2$.
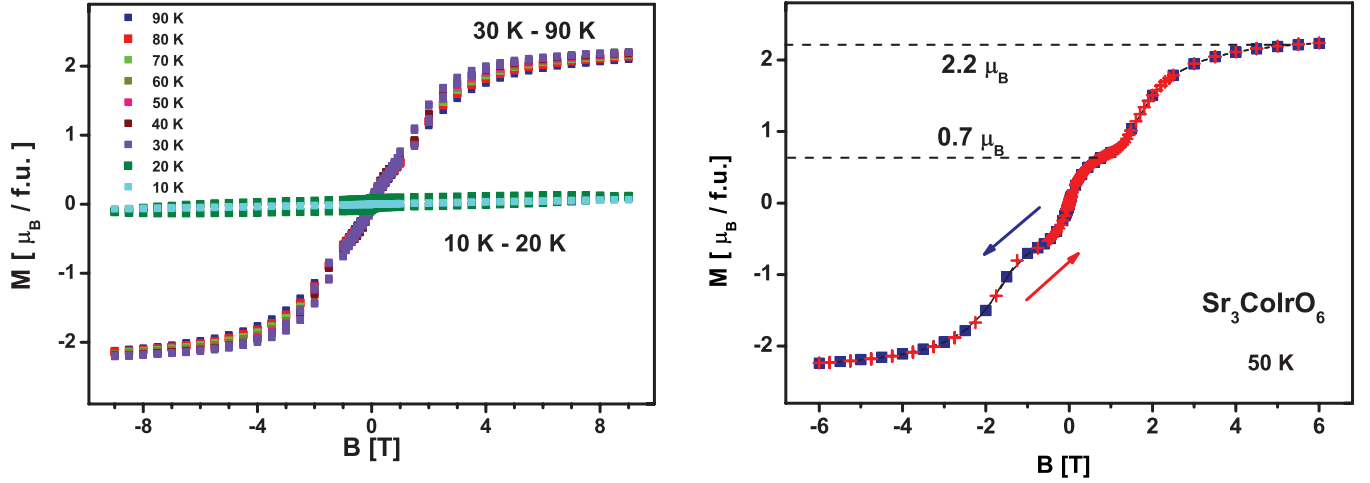
FIG. 5. (Color online) Field dependence of magnetization of Sr_3CoIrO_6 in the temperature range between 10 and 90 K (left) and at 50 K (right).

3. Time-dependent magnetic alignment in Sr_3CoIrO_6 and Sr_3NiIrO_6

Below T_2, the temperature of spin freezing at magnetic fields lower than 1 T, a frozen PDA state (F-PDA) with very slow dynamics of spins was discussed: $T_2 \sim 30$ K for Ca_3CoRhO_6,[4] $T_2 = 25$ K for Sr_3CoIrO_6, and 15 K for Sr_3NiIrO_6 (present work or 21 K[12]). Increasing temperature and magnetic field leads to magnetic phase transitions into ferri- or ferromagnetic states,[3,12] which are accompanied by the parallel orientation of spins inside individual domains and the movement of domain walls within the material. In a constant external magnetic field this domain switching is thermally activated and can be studied by measuring the magnetization as a function of time at temperatures close to T_2.

The numerous isothermal material transformations during a time interval t can be described in terms of nucleation and growth rates by the Johnson–Mehl–Avrami–Kolmogorov (JMAK) theory, for example see Ref. 32,

$$\alpha = 1 - \exp^{-kt^n}, \quad \text{or} \quad \ln[-\ln(1-\alpha)] = \ln k + n \ln t. \quad (2)$$

Here α is the fraction of the already transformed material (or in our case already aligned domains in the material), k is the growth rate constant, and n is an integer or half integer. Thus, from the time dependence of the magnetization (measured at constant temperature T and magnetic field B), one can estimate the rate constant k of spin ordering during a magnetic phase transition. Moreover, from the temperature dependence of the growth rate $k = k(T)$, the activation energy E_a for domain switching can be calculated by applying the Arrhenius equation $k = k_0 \exp(-E_a/RT)$.

Magnetization as a function of time was measured for Sr_3CoIrO_6 and Sr_3NiIrO_6 at fixed temperatures in an applied magnetic field of 6 T (Fig. 9). After each measurement at a given temperature the field was switched off, and the material was heated up to 70 K for M = Co and up to 120 K for

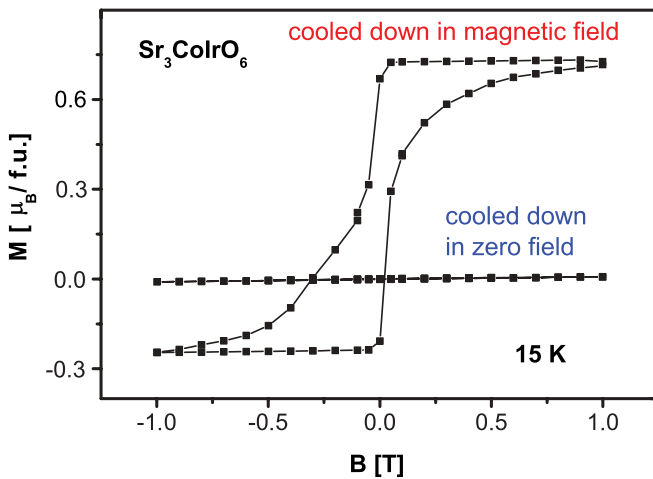FIG. 6. (Color online) Field dependence of magnetization at 15 K for Sr_3CoIrO_6 cooled down without magnetic field and cooled down in magnetic field of 1 T.
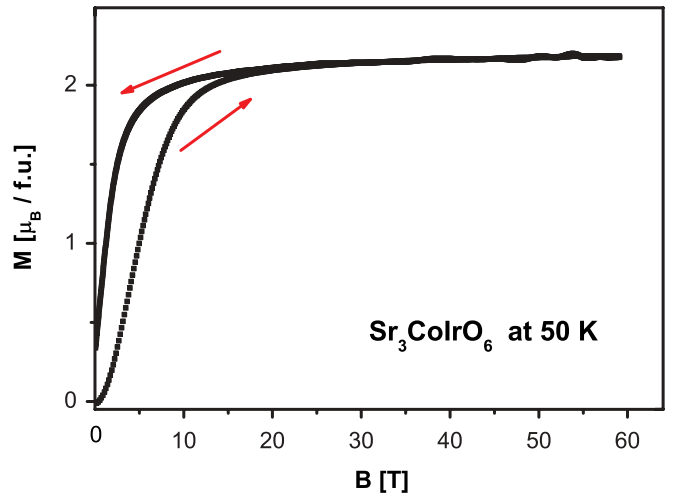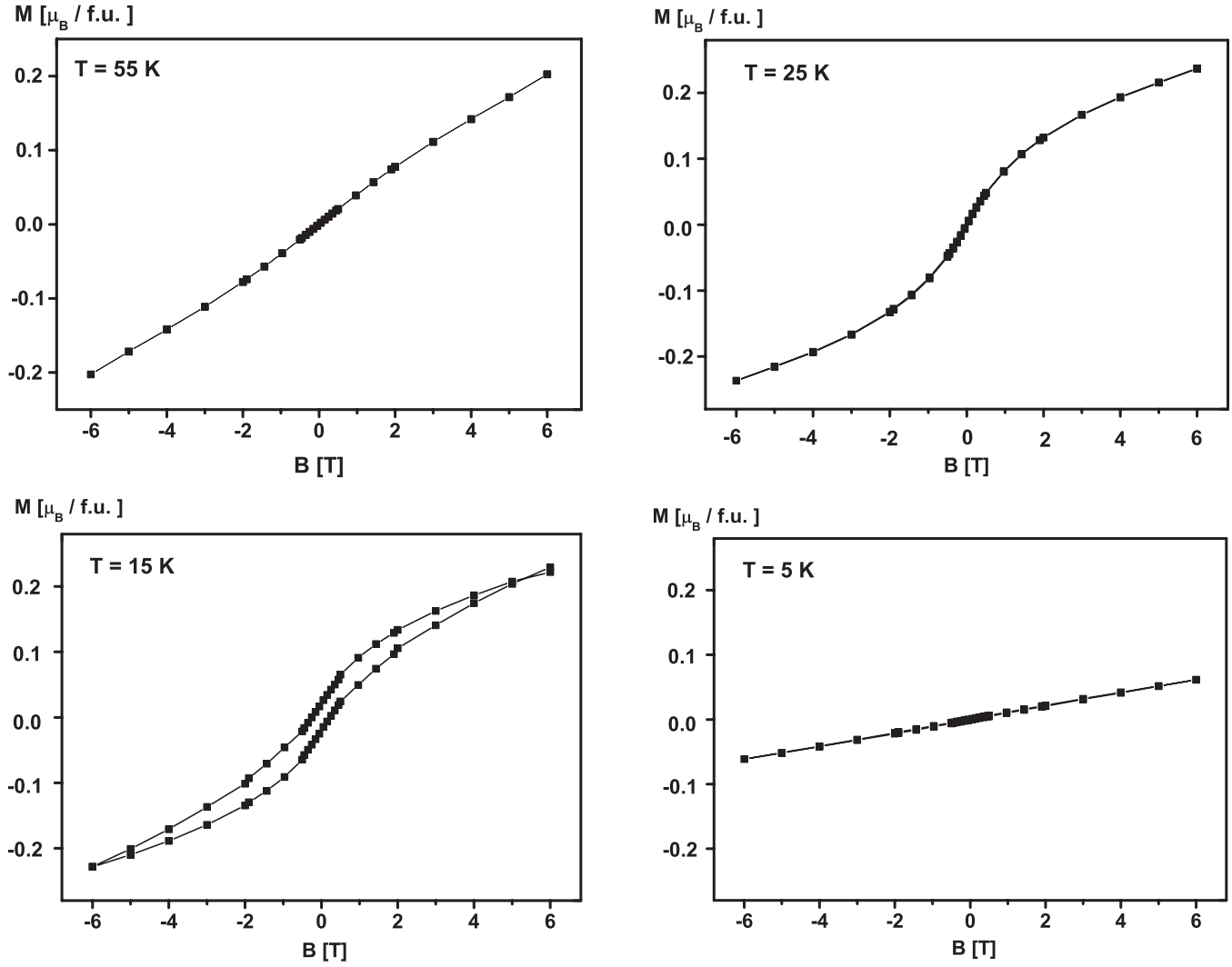

FIG. 7. (Color online) Magnetization curves of Sr_3CoIrO_6 at 50 K in pulsed magnetic fields up to 60 T. A significant hysteresis below 15 T is probably due to the slow kinetics of the reorientation of spins during the magnetic field pulses.

FIG. 8. Field dependence of the magnetization for polycrystalline Sr_3NiIrO_6 at temperatures 5–55 K.

M = Ni, in order to disorder the magnetic domains, and then cooled down to the next temperature. A saturated magnetization $M_s = 2.2$ μ_B/f.u. for the Co system and $M_s = 0.216$ μ_B/f.u. for the Ni system were used for the calculation
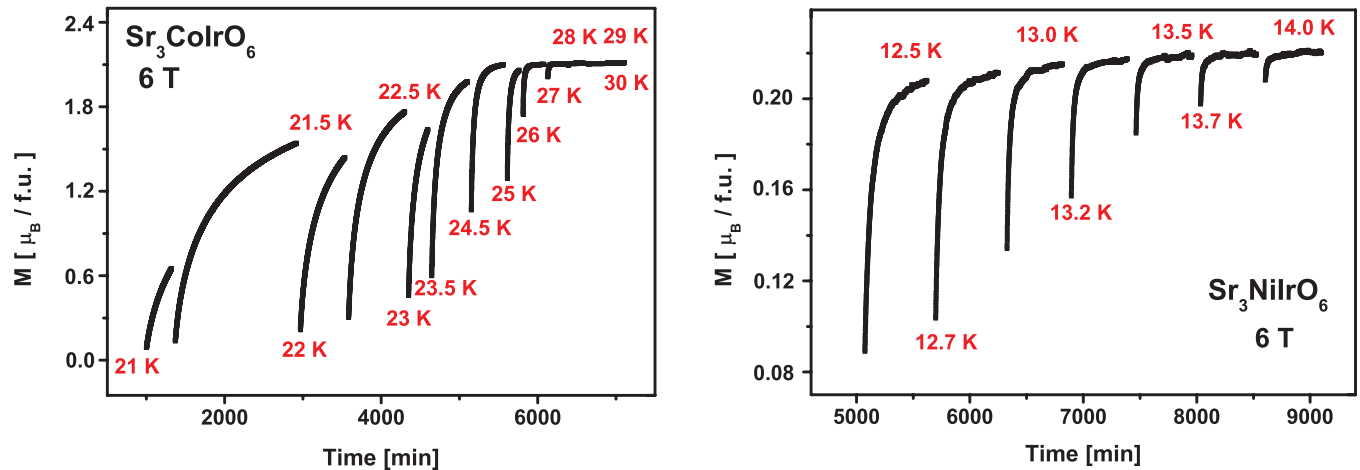

FIG. 9. (Color online) Magnetizations of $Sr_3 M IrO_6$, M = Co (left) or Ni (right) as a function of time at different temperatures in an applied magnetic field of 6 T. The magnetic domain structure was reset to the virgin state for each temperature by annealing the system in zero field at temperatures in the paramagnetic region.
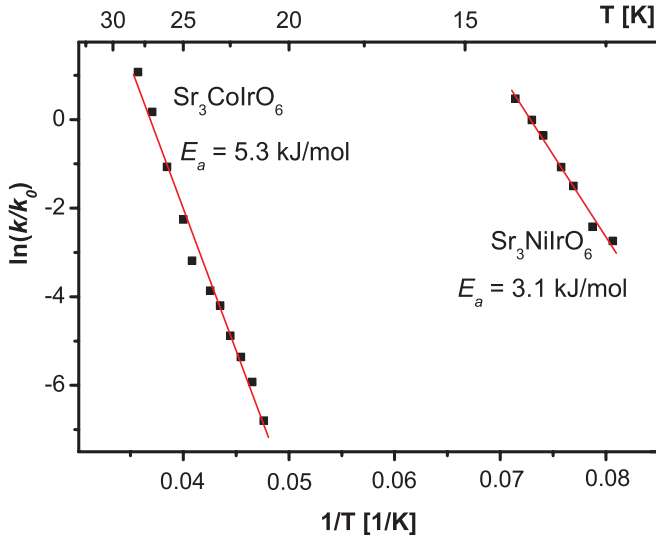
FIG. 10. (Color online) Arrhenius plot for spin ordering in Sr_3CoIrO_6 and Sr_3NiIrO_6 with k_0 [sec^n] for Sr_3CoIrO_6 and Sr_3NiIrO_6.

of $\alpha_{(t)} = M(t)/M_s$, the fraction of the already aligned domains in the sample as a function of time t. For each temperature the magnetization data were fitted by Eq. (2), and $\ln(k)$ was extracted from the linear region with n values between 0.2 and 0.6. The activation energy estimated from the Arrhenius plot for the alignment of the magnetic domains is about 5.3(3) kJ/mol, or 0.055 eV/f.u. for Sr_3CoIrO_6, and about 3.1(2) kJ/mol, or 0.032 eV/f.u. for Sr_3NiIrO_6 (Fig. 10).

4. Low-temperature synchrotron diffraction studies

The temperature dependences of the unit cell parameters of Sr_3CoIrO_6 and Sr_3NiIrO_6 are influenced by the magnetic order and, therefore, reflect the complicated magnetic behavior (see Fig. 11). Some line broadening of reflections with decreasing temperature was observed, pointing out a probable formation of local regions with a slightly distorted structure in the material. The thermal expansion coefficients for the a and c directions are positive and almost constant in the temperature region from room temperature down to the antiferromagnetic ordering temperature of about 100 K. This phonon part of the thermal expansion along a and c was estimated by a Debye function[33] with a Debye temperature for both compounds of about 300 K. For the fit modules of the McPhase modeling suite were used,[34] and only data points with $T > 100$ K were taken into account. Below this temperature the spontaneous magnetostriction leads to a zero-expansion behavior or even negative thermal expansion for both a and c for Sr_3CoIrO_6, whereas the spontaneous magnetostriction is much smaller for c in Sr_3NiIrO_6. Because of the likely large orbital moment of Co, the spontaneous magnetostriction[33] and the crystal field influence on the thermal expansion[35] of Sr_3CoIrO_6 is expected to be larger than in Sr_3NiIrO_6.

5. Heat-capacity study of the magnetic order in Sr_3CoIrO_6 and Sr_3NiIrO_6

Temperature-dependent specific heat data for Sr_3CoIrO_6 and Sr_3NiIrO_6 (Fig. 12) are monotonous, without any indication for a lambda peak, which would be expected for the onset of the long-range magnetic order. A λ peak at the magnetic transition temperature was not detected for Ca_3CoRhO_6, although a well-defined λ peak has been observed for the isostructural $Ca_3Co_2O_6$.[8] The application of an external magnetic field of 2 T does not change the heat capacity of Ca_3CoRhO_6 at temperatures close to the paramagnetic-to-ferrimagnetic transition.[8]

D. Neutron diffraction study of Sr_3CoIrO_6

1. Unpolarized neutrons

The magnetic structure of Sr_3CoIrO_6 was determined from neutron powder diffraction at 4 K (Table I).

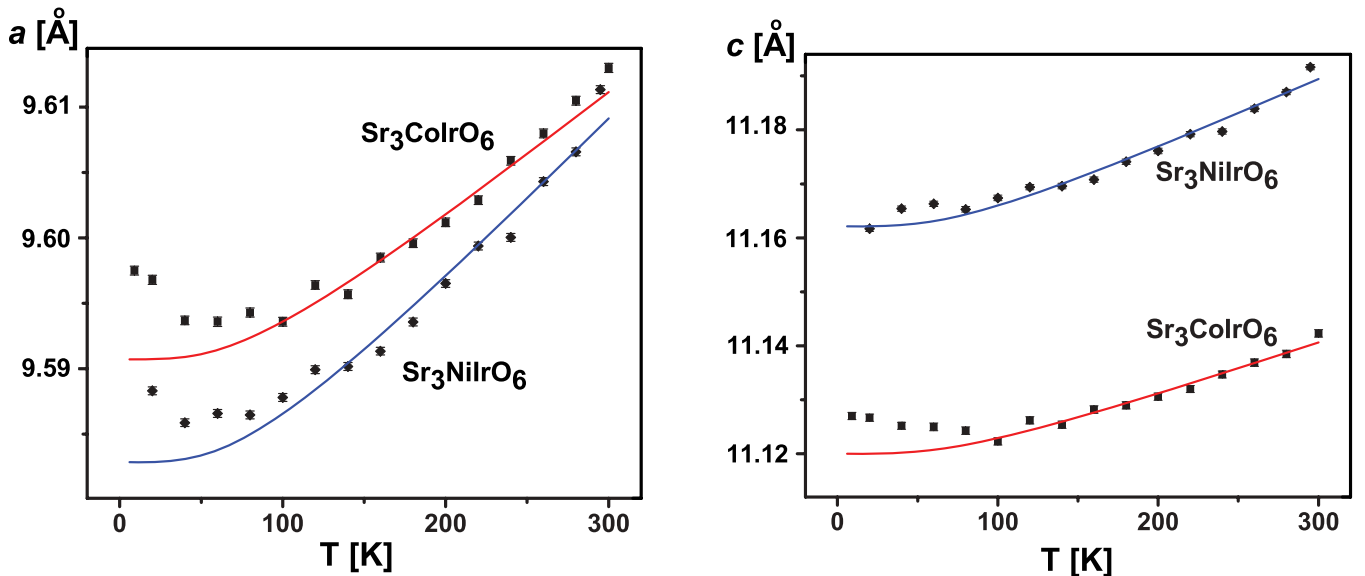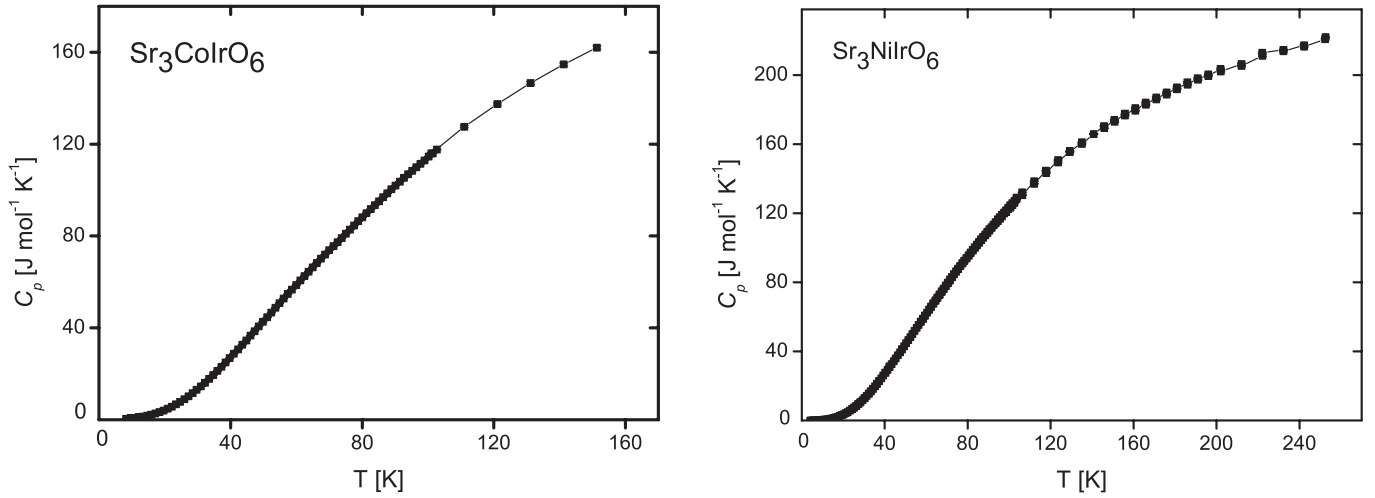FIG. 11. (Color online) Temperature evolution of the lattice parameters of Sr_3CoIrO_6 and Sr_3NiIrO_6. Lines indicate a Debye function, which is used to model the phonon part of the thermal expansion.

FIG. 12. Specific heat of Sr_3CoIrO_6 and Sr_3NiIrO_6 in zero magnetic field as a function of temperature.

No changes in the diffraction pattern were detected between 300 and 73 K, while below 73 K additional reflections with the most intense one at 2θ of about 10.5° were observed (see Fig. 13). The intensity of this magnetic reflection does not change with decreasing temperature below 36 K. Note that the full width at half maximum (FWHM) parameter for magnetic reflections is much larger than that for nuclear reflections (Fig. 14), indicating short-range order in the material. A neutron powder diffraction study of the related Ca_3CoRhO_6 compound showed additional broad diffuse magnetic intensity at the strongest magnetic Bragg reflection.[6] This effect was interpreted as the coexistence of long-range and short-

range magnetic ordering in the material. For Sr_3NiIrO_6, no magnetic reflections were identified in the neutron diffraction pattern at 10 K by comparison to the pattern at 300 K.[19]

All diffraction patterns have been analyzed by full-profile Rietveld refinements using the software package FullProf.[36] In order to eliminate the correlation between Co and Ir thermal displacement parameters B and the magnitude of magnetic moments at 4 K, the structural model was refined with fixed values B(Co) of 0.1 Å² and B(Ir) of 0.2 Å² (Table I). The mixed occupancy Ir/Co on the 6b site was also fixed to 0.97/0.03 values at 4 K.

TABLE I. Structural parameters for Sr_3CoIrO_6 at 270 K and 4 K as refined based on neutron powder diffraction data. A small excess of Co in the structure relative to Ir was revealed and quantified by 3% of Co on the Ir site. The magnetic space group for the magnetic structure was R-3.

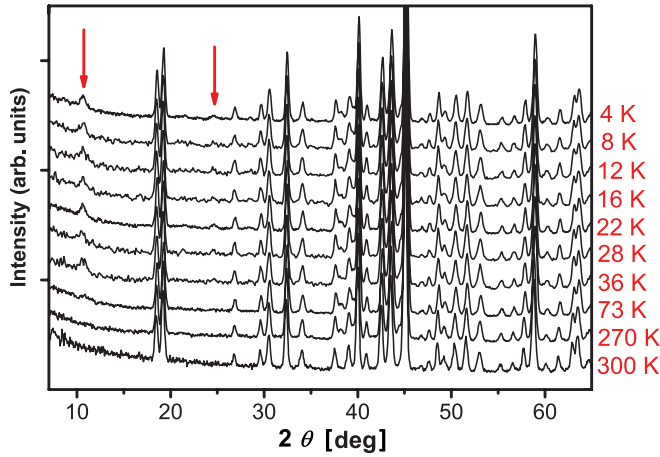|	Sr_3CoIrO_6, 270 K	Sr_3CoIrO_6, 4 K
Space group	R-3c	R-3c
a (Å), c (Å)	9.61981(7), 11.1578(2)	9.59759(9), 11.1384(2)
V (Å³)	894.22(2)	888.54(2)
Z	6	6
Sr	18e	18e
(x, y, z)	[0.3636(1), 0, 0.25]	[0.3638(1), 0, 0.25]
B (Å²)	0.56(3)	0.20(2)
Co	6a	6a
(x, y, z)	(0, 0, 0.25)	(0, 0, 0.25)
B (Å²)	0.30(9)	0.10
Ir/Co 0.97(1)/0.03(1)	6b	6b
(x, y, z)	(0, 0, 0)	(0, 0, 0)
B (Å²)	0.20(4)	0.20
O	36f	36f
(x, y, z)	[0.1727(1), 0.0203(1), 0.1132(1)]	[0.1724(1), 0.0203(1), 0.1134(1)]
B (Å²)	0.66(3)	0.32(2)
Co–O (Å)	2.1916(13)	2.1828(10)
Ir(Co)–O (Å)	2.0170(13)	2.0100(8)
$M_z(Co^{2+})$, μ_B	–	3.6(1)
$M_z(Ir^{4+})$, μ_B	–	− 0.6(2)
Bragg R factor, %	3.17	4.22
R_f factor, %	1.81	2.57

FIG. 13. (Color online) Temperature evolution of a section of the neutron diffraction patterns of Sr_3CoIrO_6 ($\lambda = 1.548$ Å).

Three different models for the magnetic structure in zero magnetic field were discussed in literature for the isostructural
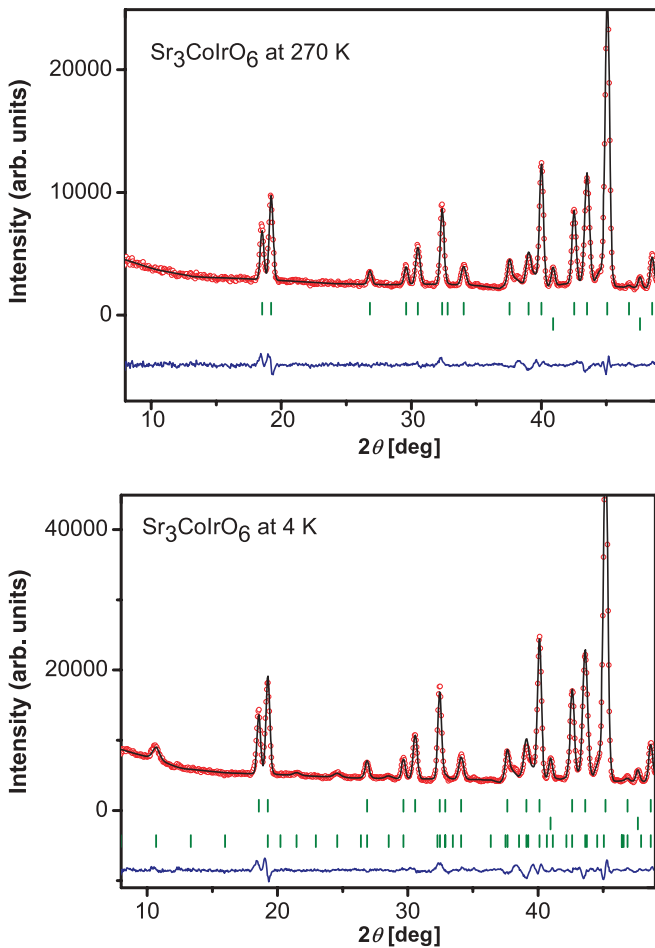

FIG. 14. (Color online) Sections of the neutron diffraction patterns of Sr_3CoIrO_6 at 270 K and 4 K (lower 2θ region). The positions of the magnetic Bragg reflections at 4 K are shown by the lower line of marks for the "$+M, -M/2, -M/2$" structure model. The other marks indicate the Bragg reflections from the crystal structure (top) and 0.8% (w/w) Ir (middle).

$Ca_3Co_2O_6$ and Ca_3CoRhO_6 compounds: (i) an incommensurate amplitude modulated antiferromagnet[2]; (ii) the PDA,[3,4] where 2/3 of magnetic chains order antiferromagnetically and the other 1/3 are disordered; and (iii) a ferrimagnetic structure with 2/3 of the magnetic chains ferromagnetically and the other 1/3 antiferromagnetically aligned.[1] In addition, the short-range magnetic order of Co^{2+} ions, as revealed by the diffuse character of the magnetic 100 reflection, was proposed.[6] It is an extremely difficult task to draw unambiguous conclusions from a powder diffraction pattern in these kinds of systems. This is demonstrated by the highly complex modulated PDA structure with a very long periodicity, which was revealed for $Ca_3Co_2O_6$ based on high-resolution magnetic x-ray scattering.[37]

A ferrimagnetic order of the interchain spin arrangement in the ab plane can be ruled out for Sr_3CoIrO_6, because no significant change of intensity of the nuclear reflections is observed below the magnetic transition. This is consistent with the very low moment seen in the ZFC magnetization data [Fig. 4(a)]. A Rietveld refinement of the nuclear structure confirms that the Ir- and Co-ions are located on octahedral and trigonal-prismatic coordinated sites, respectively (Table I). Two different magnetic structure models were considered in order to explain the magnetic reflections below 73 K: (i) a commensurate modulated antiferromagnetic structure[2] with the propagation vector $\mathbf{k} = (0, 0, 1)$ in the space group R-3; and (ii) the PDA $(+M, -M, 0)$ structure[6] with the propagation vector $\mathbf{k} = (0, 0, 0)$ in the space group P-3.[1]

An incommensurate modulated antiferromagnetic structure with propagation vector $\mathbf{k} = (0, 0, k_z)$ has been also considered. In fact $(0, 0, 1)$ is not a special point of the Brillouin zone, and a small incommensurate propagation vector $(0, 0, 1.01)$, corresponding to a very long modulation, was observed in $Ca_3Co_2O_6$.[2,37] However, given the limited resolution of our powder diffraction data we can determine k_z to be $k_z = 1.00 \pm 0.01$ and therefore use $\mathbf{k} = (0, 0, 1)$ in the following discussion.

The magnetic form factor of iridium has been approximated by that of Rh.[38]

Both magnetic models (i) and (ii) can excellently describe the magnetic reflections with nearly similar magnetic moments on the iridium site [0.6(1)–0.7(1) μ_B/f.u.] and cobalt site [3.3(1) or 3.6(1) μ_B/f.u.] and very similar residuals at 4 K. The commensurate antiferromagnetic structure (i) with $\mathbf{k} = (0, 0, 1)$ is supported for Sr_3CoIrO_6 by the following three considerations: (1) a modulated antiferromagnetic structure with R-3 exhibits higher symmetry in comparison to the P-3 one of the PDA; (2) magnetizations in a low magnetic field above $T_2 = 30$ K are close to zero [see Fig. 4(a)], which is too low for a PDA state with 1/3 of the chains in the structure being randomly oriented; and (3) the critical magnetic field strength of 1 T for the first field-induced magnetic phase transition into a ferrimagnetic state at 50 K (see Fig. 5) seems too high for a spin reorientation in the incoherent magnetic chains of the PDA.

The magnetic structure has been analyzed using the standard irreducible representation theory for the propagation vector $\mathbf{k} = (0, 0, 1)$. Only the symmetry-adapted mode belonging to the irreducible representation $\Gamma 1$ allows a fit to the data. The magnetic moments for Co and Ir ions located at the $6a$ $(0, 0, 1/4)$ and $6b$ $(0, 0, 0)$ sites, respectively, are given by
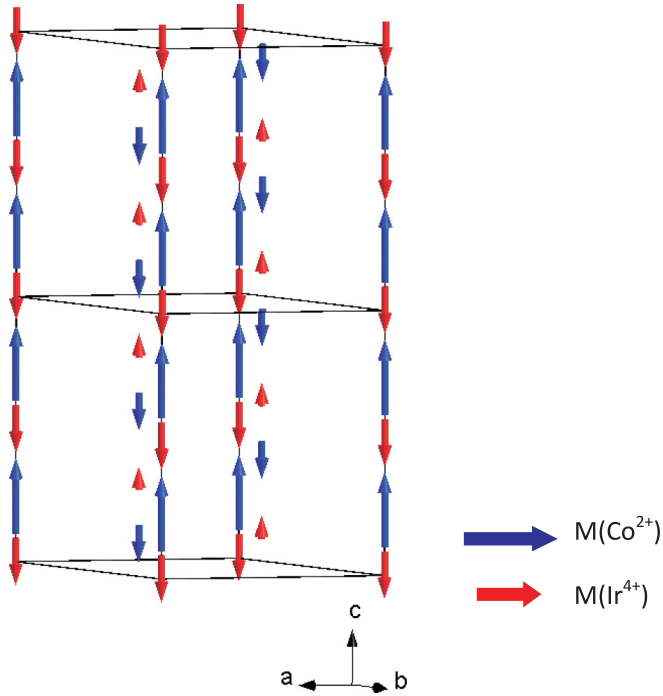
FIG. 15. (Color online) A commensurate, modulated antiferromagnetic structure of Sr_3CoIrO_6 with the propagation vector $\mathbf{k} = [0, 0, 1.00(1)]$. The arrangement of the ordered magnetic moments in the ab plane can be described as $(M, -M/2, -M/2)$.

$\mathbf{M_{j=a,b}}(\mathbf{R_L}) = \mathbf{M_j} \cos(2\pi \mathbf{k} \cdot \mathbf{R_L})$. Here the Fourier coefficients $\mathbf{M_a}$ and $\mathbf{M_b}$ correspond to the maximum magnetic moments at the $6a$ and $6b$ sites, respectively, and $\mathbf{R_L}$ is the translation vector with respect to the zero$^{\text{th}}$ cell. All magnetic moments are aligned parallel to the c axis. Using the noninteger translations inside the magnetic unit cell $t_1 = (2/3, 1/3, 1/3)$ and $t_2 = (1/3, 2/3, 2/3)$, one can see that there is a phase shift of $120°$ in the magnetic moment between adjacent chains. Consequently, the arrangement of the ordered magnetic moments in the ab plane can be described as $(M, -M/2, -M/2)$, where the labels in parenthesis indicate the relative magnetizations on the triangular network formed by the chains. Note that the relevant phase factors are $\cos(2\pi/3) = \cos(4\pi/3) = -1/2$.

A scheme of the magnetic structure is shown in Fig. 15. This type of structure is usually induced by competing exchange interactions in the presence of strong axial anisotropy, stabilizing an arrangement in which the ordered component of the magnetic moment fluctuates along the propagation direction. The refined values of the magnetic Co moment of 3.6(1) μ_B and Ir moments of $-0.6(1)$ μ_B do not depend significantly on temperature between 4 K and 36 K within the available resolution of the diffraction data.

The 3.6 μ_B value for the Co^{2+} is larger than the spin-only value of 3 μ_B for an $S = 3/2$ ion and indicates, therefore, the presence of orbital moment on the Co.

2. Polarized neutrons

Measured intensities recorded by diffraction with polarized neutrons are shown in Fig. 16. The nuclear contributions, as derived from the polarization analysis of data collected at 4 and 80 K, are very similar, indicating that no structural phase transition of Sr_3CoIrO_6 takes place in this temperature range. The nearly temperature-independent incoherent scattering increases nonlinear with Q and exhibits a maximum at ~ 2.2 Å^{-1}. The magnetic contribution at 4 K yields a clear peak at $Q = 0.75$ Å^{-1}, which is not visible at 80 K and should be related to the magnetic order in Sr_3CoIrO_6. Nevertheless, the shape of the magnetic contribution at 4 K and 80 K is far from linear, i.e., two broad maxima at 0.75 and 1.75 Å^{-1} were observed, thus indicating the presence of a diffuse magnetic signal, probably due to short-range magnetic order above and below the magnetic ordering temperature, similar to Ca_3CoRhO_6.[6]

IV. CONCLUSION

We find that the magnetic behavior of Sr_3CoIrO_6 resembles more that of Ca_3CoRhO_6 with the same spin states of cations in MO_6 trigonal prisms and $M'O_6$ octahedra than that of Sr_3NiIrO_6 with Ni^{2+} ($S = 1$) and quenched orbital moment. All three compounds have two characteristic temperatures T_1 and T_2, which separate spin freezing at very low temperature (below T_2) and an intermediate temperature region ($T_2 < T < T_1$) with field-induced magnetic transitions and the paramagnetic region at higher temperatures (above T_1). Sr_3CoIrO_6 shows nearly the same transition temperature $T_1 = 90$ K as Ca_3CoRhO_6, and the analysis of the inverse paramagnetic susceptibility indicates a similar size of the magnetic interactions in both compounds in spite of the larger Sr
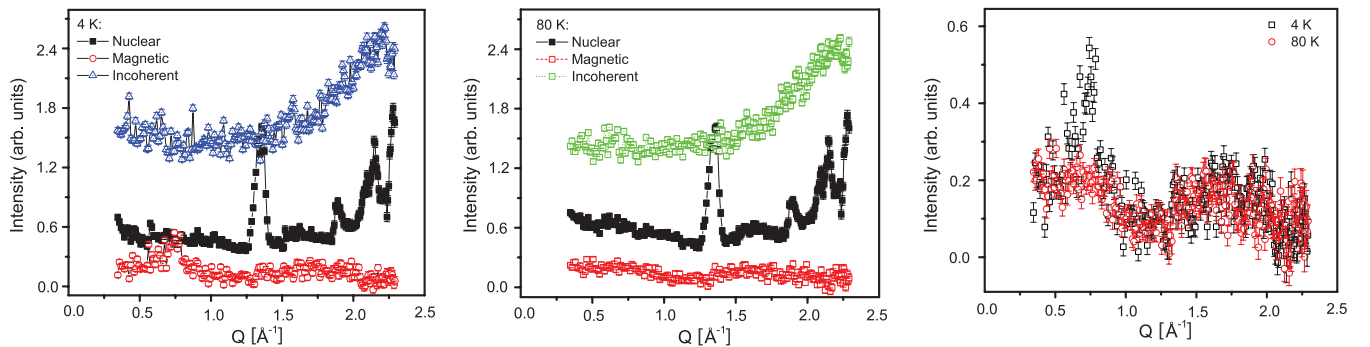

FIG. 16. (Color online) Different contributions to the diffraction patterns of Sr_3CoIrO_6 at (a) 4 K and (b) 80 K together with a comparison of the extracted magnetic contributions at (c) both temperatures.

atoms between the Co chains and, therefore, longer Co-Co interchain distances in Sr_3CoIrO_6. The complex magnetic order below the transition temperature T_1 influences the thermal behavior of the lattice parameters of Sr_3CoIrO_6 and Sr_3NiIrO_6: both a and c parameters in Sr_3CoIrO_6 show pronounced magnetoelastic effects, whereas the spontaneous magnetostriction for c parameter in Sr_3NiIrO_6 is smaller.

Similar to Ca_3CoRhO_6, between T_1 and T_2 Sr_3CoIrO_6 seems to become purely ferromagnetic by a spin-flip transition at rather moderate external fields of 4–5 T. The magnetization of Sr_3NiIrO_6 is linear, and no saturation is observed in fields up to 7 T.

Powder neutron diffraction data of Sr_3CoIrO_6 and Ca_3CoRhO_6 in zero field can be interpreted successfully by either a pure antiferromagnetic or a PDA state. Below 100 K, neutron diffraction in an applied magnetic field of 2 T revealed a ferrimagnetic structure for Ca_3CoRhO_6,[4] which corresponds to the first plateau in the field dependence of magnetization. A similar ferrimagnetic structure could be expected for Sr_3CoIrO_6, showing also a plateau at 50 K and about 1 T. Magnetic Bragg reflections were not observed in the neutron powder diffraction pattern of Sr_3NiIrO_6.[19] Note,

that the isostructural Ca_3CoIrO_6 compound with a shorter Co-Co interchain distance in comparison to Sr_3CoIrO_6 shows a higher degree of frustration, leading to a dominant short-range magnetic order and the absence of significant contributions to magnetic Bragg reflections in neutron powder diffraction patterns at low temperatures.

Our low-temperature neutron powder diffraction data provided indications for the presence of an orbital magnetic moment of Co in Sr_3CoIrO_6. We also argue that parts of the sample might show order after a long relaxation time as magnetic reflections of such one-dimensional oxides exhibit clear time dependence.[39] For example, a time-dependent magnetic transition from one long-range ordered state to another in a zero magnetic field, occurring over a time interval of several hours, was observed for $Ca_3Co_2O_6$.[39]

[1] S. Aasland, H. Fjellvag, and B. Hauback, Solid State Commun. **101**, 187 (1997).

[2] S. Agrestini, L. C. Chapon, A. Daoud-Aladine, J. Schefer, A. Gukasov, C. Mazzoli, M. R. Lees, and O. A. Petrenko, Phys. Rev. Lett. **101**, 097207 (2008).

[3] S. Niitaka, H. Kageyama, K. Yoshimura, K. Kosuge, S. Kawano, N. Aso, A. Mitsuda, H. Mitamuda, and T. Goto, J. Phys. Soc. Jpn. **70**, 1222 (2001).

[4] S. Niitaka, K. Yoshimura, K. Kosuge, M. Nishi, and K. Kakurai, Phys. Rev. Lett. **87**, 177202 (2001).

[5] E. V. Sampathkumaran and A. Niazi, Phys. Rev. B **65**, 180401(R) (2002).

[6] M. Loewenhaupt, W. Schäfer, A. Niazi, and E. V. Sampathkumaran, Europhys. Lett. **63**, 374 (2003).

[7] H. Wu, Z. Hu, D. I. Khomskii, and L. H. Tjeng, Phys. Rev. B **75**, 245118 (2007).

[8] V. Hardy, M. R. Lees, A. Maignan, S. Hébert, D. Flahaut, C. Martin, and D. McK Paul, J. Phys.: Condens. Matter **15**, 5737 (2003).

[9] H. Kageyama, K. Yoshimura, and K. Kosuge, J. Solid State Chem. **140**, 14 (1998).

[10] S. Rayaprol, K. Sengupta, and E. V. Sampathkumaran, Phys. Rev. B **67**, 180404 (2003).

[11] N. Mohapatra, K. K. Iyer, S. Rayaprol, and E. V. Sampathkumaran, Phys. Rev. B **75**, 214422 (2007).

[12] D. Flahaut, S. Hébert, A. Maignan, V. Hardy, C. Martin, M. Hervieu, M. Costes, B. Raquet, and J. M. Broto, Eur. Phys. J. B **35**, 317 (2003).

[13] G. R. Zhang, X. L. Zhang, T. Jia, Z. Zeng, and H. Q. Lin, J. Appl. Phys. **107**, 09E120 (2010).

[14] X. X. Wang, J. J. Li, Y. G. Shi, Y. Tsujimoto, Y. F. Guo, S. B. Zhang, Y. Matsushita, M. Tanaka, Y. Katsuya, K. Kobayashi, K. Yamaura, and E. Takayama-Muromachi, Phys. Rev. B **83**, 100410 (2011).

[15] H. Wu, M. W. Haverkort, Z. Hu, D. I. Khomskii, and L. H. Tjeng, Phys. Rev. Lett. **95**, 186401 (2005).

[16] T. Burnus, Z. Hu, M. W. Haverkort, J. C. Cezar, D. Flahaut, V. Hardy, A. Maignan, N. B. Brookes, A. Tanaka, H. H. Hsieh, H.-J. Lin, C. T. Chen, and L. H. Tjeng, Phys. Rev. B **74**, 245111 (2006).

[17] T. Burnus, Z. Hu, H. Wu, J. C. Cezar, S. Niitaka, H. Takagi, C. F. Chang, N. B. Brookes, H.-J. Lin, L. Y. Jang, A. Tanaka, K. S. Liang, C. T. Chen, and L. H. Tjeng, Phys. Rev. B **77**, 205111 (2008).

[18] D. Mikhailova, N. Narayanan, W. Gruner, A. Voss, A. Senyshyn, D. M. Trots, H. Fuess, and H. Ehrenberg, Inorg. Chem. **49**, 10348 (2010).

[19] T. N. Nguyen and H.-C. zur Loye, J. Solid State Chem. **117**, 300 (1995).

[20] D. Eckert, R. Grössinger, M. Doerr, F. Fischer, A. Handstein, D. Hinz, H. Siegel, P. Verges, and K.-H. Müller, Physika B **294–295**, 705 (2001).

[21] M. Knapp, C. Baehtz, H. Ehrenberg, and H. Fuess, J. Synchrotron Rad. **11**, 328 (2004).

[22] M. Knapp, V. Joco, C. Baehtz, H. H. Brecht, A. Berghaeuser, H. Ehrenberg, H. von Seggern, and H. Fuess, Nucl. Instrum. Meth. A **521**, 565 (2004).

[23] M. Hoelzel, A. Senyshyn, R. Gilles, H. Boysen, and H. Fuess, Neutron News **18**, 23 (2008).

[24] O. Schaerpf and H. Capellmann, Phys. Status Solidi A **135**, 359 (1993).

[25] A. D. Hillier, D. T. Adroja, W. Kockelmann, L. C. Chapon, S. Rayaprol, P. Manuel, H. Michor, and E. V. Sampathkumaran, Phys. Rev. B **83**, 024414 (2011).

[26] R. C. Layland and H.-C. zur Loye, J. Alloys Compd. **299**, 118 (2000).

[27] T. Pauporte, D. Aberdam, J.-L. Hazemann, R. Faure, and R. Durand, J. Electroanal. Chem. **465**, 88 (1999).

[28] M. Hüppauff and B. Lengeler, J. Electrochem. Soc. **140**, 598 (1993).

[29] D. Y. Jung, G. Demazeau, and J. H. Choy, J. Mater. Chem. **5**, 517 (1995).

[30] T. Burnus, Z. Hu, H. H. Hsieh, V. L. J. Joly, P. A. Joy, M. W. Haverkort, H. Wu, A. Tanaka, H.-J. Lin, C. T. Chen, and L. H. Tjeng, Phys. Rev. B **77**, 125124 (2008).

[31] S. Niitaka, H. Kageyama, M. Kato, K. Yoshimura, and K. Kosuge, J. Solid State Chem. **146**, 137 (1999).

[32] M. C. Weinberg, D. P. Birnie, III, and V. A. Shneidmann, J. Non-Cryst. Solids **219**, 89 (1997).

[33] A. Lindbaum and M. Rotter, in *Ferromagnetic Materials*, edited by K. H. J. Buschow and E. P. Wohlfarth, Vol. 14 (Elsevier Sci. Pub., Amsterdam, The Netherlands, 2002), pp. 307–362.

[34] www.mcphase.de, M. Rotter, J. Magn. Magn. Mater. **272–276**, 481 (2004).

[35] E. Gratz, M. Rotter, A. Lindabum, H. Müller, E. Bauer, and H. Kirchmayr, J. Phys.: Condens. Matter **5**, 567 (1993).

[36] T. Roisnel and J. Rodriguez-Carvajal, Mater. Sci. Forum **378–381**, 118 (2001).

[37] S. Agrestini, C. Mazzoli, A. Bombardi, and M. R. Lees, Phys. Rev. B **77**, 140403(R) (2008).

[38] P. J. Brown, in *International Tables for Crystallography*, edited by E. Prince, Vol. C (Kluwer Acad. Pub., Dordrecht, The Netherlands, 2004), pp. 454–460.

[39] S. Agrestini, C. L. Fleck, L. C. Chapon, C. Mazzoli, A. Bombardi, M. R. Lees, and O. A. Petrenko, Phys. Rev. Lett. **106**, 197204 (2011).